Romanian Reports in Physics **XX**, XYZ (2017)

MONITORING DROPLET EVAPORATION VIA REAL-TIME DIGITAL HOLOGRAPHIC INTERFEROMETRY USING A PHASE ONLY SPATIAL LIGHT MODULATOR

A. SIMA[1], P. C. LOGOFĂTU[2*], M. L. PASCU[2], I. NICOLAE[2]

[1] University "Politehnica" of Bucharest, Faculty of Electronics, Telecommunications and Information Technology, Bd. Iuliu Maniu 1-3, Bucharest, Romania
E-mail: adriansima1981@gmail.com,
[2] National Institute for Laser, Plasma and Radiation Physics, Laser Dept., str. Atomi□tilor nr. 409, CP MG-36, Măgurele, jud. Ilfov, Romania, 077125, E-mail: petre.logofatu@inflpr.ro,
E-mail: mihai.pascu@inflpr.ro, E-mail: ionut.nicolae@inflpr.ro.
[*]Corresponding author: P. C. Logofătu

Received

Abstract. A previous attempt to use interferometry to investigate the modifications in shape and refractive index within a water droplet using a plane-parallel light wave has failed. We report success, however, when using a divergent wave. Additional advantages are derived from the use of a dynamic digital holographic arrangement that can perform real-time observation of the optical path modifications induced by the droplet evaporation. Holograms are recorded on a digital camera sensor, subtracted from the initial hologram and displayed on a spatial light modulator that, under illumination, performs the optical reconstruction of a real-time holographic interferometry "motion picture". For comparison and fitting the phenomenon was mathematically modelled in the geometric approximation. Qualitative agreement was demonstrated. The extension of the technique to the measurement of more complex phenomena, such as the perturbation of the droplet by inelastic or elastic interaction with a pulsed laser is straightforward.

Key words: holographic interferometry, optofluidics, geometric approximation.

1. INTRODUCTION

Water droplets are used extensively in technological and biological applications [1,2]. Optical and laser methods of investigating the droplets are part of the relatively newly constituted field of optofluidics. These methods are often preferred for being non-contact. In a previous study [3] we have shown that it is not possible to investigate the modifications in shape and refractive index within a water droplet via interferometric means if the instrument used for investigation is a plane-parallel wave. Things are different, however, if we use a divergent beam as an instrument of investigation. The use of divergent beams in interferometry is not new [4,5], but this particular experimental arrangement for this particular purpose

is original, to the best of our knowledge. Additional advantages are drawn from the use of a dynamic digital holographic arrangement which can perform real-time observation of the optical path modifications induced by the droplet evaporation. Any changes in the optical path due to evaporation (or any other factors) can be observed in real-time in the dynamic fringe pattern generated through SLM reconstruction. For comparison and fitting, the evolution of the fringe pattern induced by the droplet evaporation was calculated theoretically using a geometric approximation model. This experimental arrangement is a modified and improved version of a series of arrangements for real-time investigation of phase objects presented in several previous papers [6-8].

In this paper, we used this holographic arrangement to monitor the droplet evaporation, but the extension of the technique to the study of more complex phenomena, such as the perturbation of the droplet by inelastic or elastic interaction with a pulsed laser is straightforward.

2. EXPERIMENTAL ARRANGEMENT

2.1 PLANE-PARALLEL VS. DIVERGENT BEAM

We previously tried to characterize the water droplet using a plane-parallel beam and a Mach-Zehnder interferometer [3]. The attempt failed for reasons best understood if one looks at Fig. 1.(a). A plane-parallel wave is scattered by the droplet at large angles outside the shadow area of the droplet. The image of the droplet is distorted beyond recognition and drowned in the spurious information coming from diffraction of the light at the edges of the droplet. However, things change if we use a divergent beam, as one can see in Fig. 1.(b). The beam is scattered to a great extent within the shadow area of the droplet. The figure of the droplet is inverted, but it is less distorted, and confined within a reasonably small space that can be adjusted from the divergence angle. Also, the diffraction at the edges is now sent away at large angles, most of it outside the shadow of the droplet. There is an intuitive correspondence between the interferogram and the droplet. In the tracing of the rays from Fig. 1 and throughout this paper the geometric approximation treatment was used for simplicity.

2.2 HOLOGRAPHIC INTERFEROMETRY EXPERIMENTAL ARRANGEMENT

The holographic interferometry experimental arrangement used in this work (see Fig. 2) has two stages: the recording stage in the far side, which uses as

coherent light source the He-Ne laser, and the reconstruction stage in the near side, which uses as source a Nd:YAG laser.

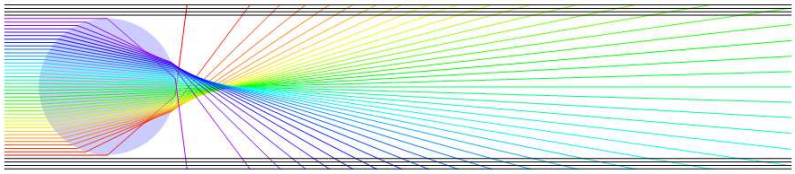

(a)

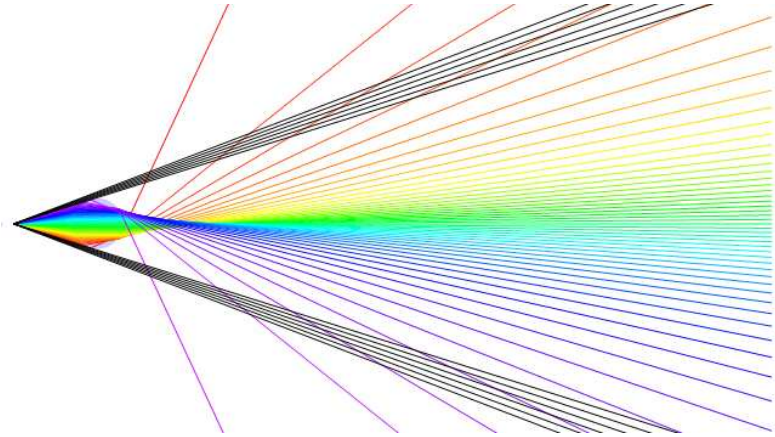

(b)

Fig. 1 - A plane-parallel beam is scattered by a water droplet (a). A divergent beam is scattered by a water droplet (b). The light is propagating from left to right. A colour code was used for rays to facilitate the tracking of the rays, namely the rays were coloured from red to violet, starting from the bottom.

In the recording stage, the He-Ne laser beam is spatially filtered and collimated, then directed toward lens L, which turns the plane-parallel beam into a divergent beam. This divergent beam is then refracted by the droplet to the white diffusive screen Sc. The screen is the object whose hologram is recorded by the CCD. The phase distribution of the light at the screen contains information about the changing shape of the droplet and of the refractive index distribution inside the droplet. The lens L images the screen somewhere in the region of the beam splitter BS and it is the Fresnel transform of this image that reaches the CCD, together with the reference beam directed there by the mirrors M1, M2 and the beam splitter. Therefore, we are dealing with Fresnel holograms. There is a slight tilt between the reference and the object beams; the tilt is necessary for the holograms to be off-axis and the slightness is dictated by the low resolution of the CCD.

Note that the elements L and WD play two quite different roles pending on the propagation direction of the light. In the first pass of the light, from BS toward

Sc, L turns the collimated beam into a divergent beam that passes almost entirely through WD and then reaches Sc as a wavefront with an approximately simple spherical shape. In the second pass, from Sc to BS, WD has almost no effect on the very complex wavefront diffused by Sc, being too little, and L acts as an imaging lens for the object Sc. This aspect ensures the compactness of the arrangement. Another important aspect to note is the fact that we are dealing here with a Michelson-type configuration that ensures for the object Sc a position external to the bulk of the arrangement. This position can accommodate a variety of dimensions and shapes for the object. This aspect ensures the versatility of our arrangement. Its compactness and versatility makes this arrangement especially suitable for technological and industrial applications.

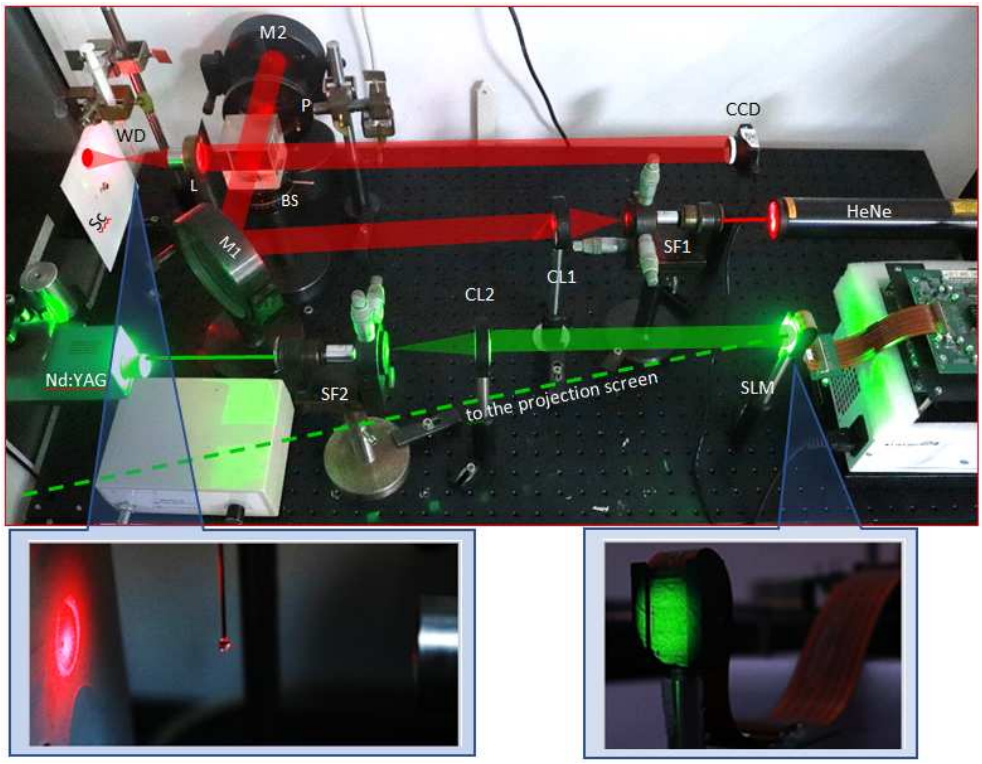

Fig. 2 - Holographic interferometry arrangement. HeNe stands for polarized He-Ne laser (633 nm); Nd:YAG for Nd:YAG second harmonic laser (532 nm); SF for spatial-filter; CL for collimating lens; M for mirror; P for polarizer (light attenuator); BS for beam-splitter cube; WD for water droplet; Sc for white diffusive screen.

In the reconstruction (or the playback) part, the beam is spatially filtered and collimated, then sent to a phase only spatial light modulator (SLM). The SLM diffracts the light to a projection screen not shown in the figure. The whole system

is controlled by a computer program that uses the holograms recorded by the CCD in the following manner: It keeps the first hologram as reference, subtracts from it the ensuing holograms, and then sends the subtraction to the SLM. The subtraction is the digital equivalent of a holographic interferogram. Also, since the intensities recorded by the CCD are converted into phases by the SLM, the digital equivalent of a bleaching is performed. By adjusting the position of the lens CL2 one can focus the image of the interferogram on the projection screen. One sees on this screen a real-time "motion picture" of the evolution of the interferogram.

This type of reconstruction stage has several advantages. It permits a real-time observation of the interferogram as in an analogous arrangement while retaining all the advantages of a digital arrangement. The "bleaching" performed by the SLM ensures the brightness of the image. The subtraction of the holograms eliminates the spurious information related to the imperfections of the screen or the beam and leaves only the phase differences due to changes in the state of the droplet.

Even without doing anything to the droplet, the simple evaporation process already causes visible changes of the interferogram. This testifies for the sensitivity of the arrangement. In this work the evaporation of the droplet was the only type of change of the droplet state that was studied.

3. GEOMETRIC APPROXIMATION MODEL FOR CALCULATING THE HOLOGRAFIC INTERFEROGRAM "MOTION PICTURE"

The theoretical difficulties of a rigorous treatment of the physical phenomena that take place in this experiment, combined with the convenient simplification of creating interferograms by mathematical subtraction, led us to assume great simplifications in the theoretical calculation of the interferograms. We used the geometric approximation, which we know is not very good for the edges of the sphere [9]. We also neglected the amplitude, and we dealt with phase only. We simply assumed amplitude to be unity everywhere. The "bleaching" is a partial justification for this simplification. The derivations were still quite laborious, for which reason we show here only some highlights. We assumed that the SLM reproduces at the projection screen precisely the phase distribution at the screen Sc.

For a geometry as shown in Fig. 3, it is natural to use three reference systems: a static one attached to Earth (S) and two moving ones, attached to the droplet (S' and S"). (Figs 3-5 are not just illustrations, they represent rigorous calculations.) All three have the focal point F of lens L, where the waist of the divergent beam is located, on the *z* axis. The relation between the three reference systems is best seen in Fig. 4. S' is obtained from S by a translation on the *x* axis, so that the centre of the droplet becomes the origin of the system, and a rotation

with ξ about the *y* axis, so that F is located again on the *z*' axis. The system S" is obtained from S' by a rotation with φ about the axis *z*', so that the ray FBGW is contained in the *x*"*z*" plane. Choosing these reference systems simplifies the formulae considerably.

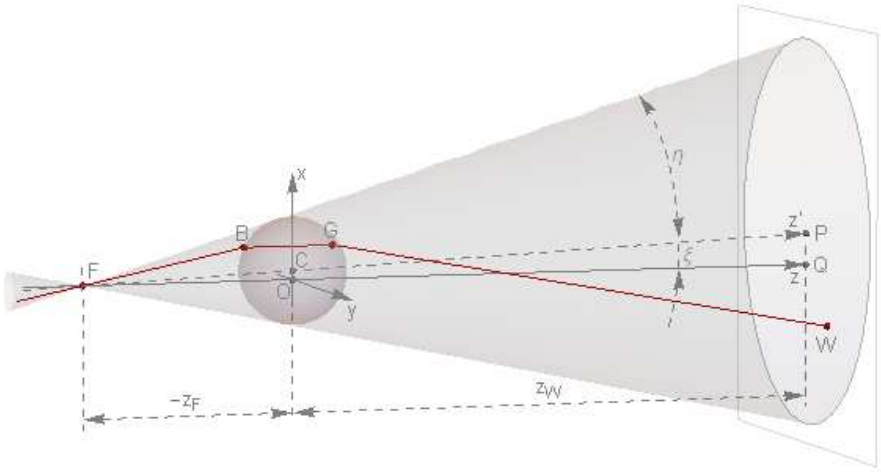

Fig. 3 - Illustration of the general configuration of the divergent beam, the droplet and the screen. F is the point where the waist of the beam is located, C the centre of the sphere, FBGW is an example of ray tracing corresponding to an inclination θ' and azimuth φ of the ray.

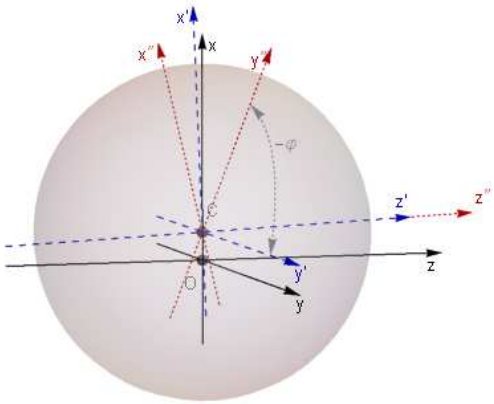

Fig. 4 – Zoom on the droplet, which illustrates the three reference systems used in the analytical derivations.

The tilt of the *x*' and *z*' with respect to the *x* and *z* changes during the evaporation of the droplet and has the expression

$$\xi = \arctan\left(\frac{x_C}{-z_F}\right). \tag{1}$$

where $-z_F$ is the distance from O to F, and x_C is variable. In the reference system S', the distance from C to F is

$$z'_F = -\sqrt{{x_C}^2 + {z_F}^2}\,. \tag{2}$$

Then, the maximum angle which a ray that enters the droplet may make with the z' axis, when it is tangent to the sphere, is

$$\eta = \arcsin\left(\frac{R}{-z'_F}\right). \tag{3}$$

The projection of the sphere from the focal point F onto the wall is an ellipsis.

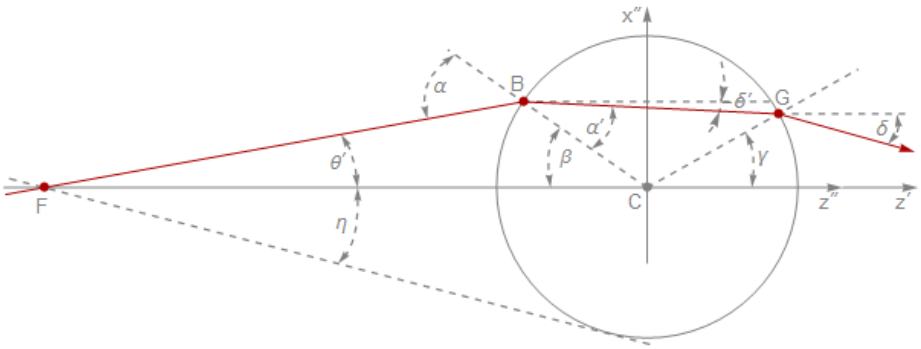

Fig. 5 - Longitudinal section of the system containing the plane x"z", without the screen, illustrating the trajectory of the beam through the sphere and the main geometric elements used in the derivation of the formulae.

In order to calculate the interferogram, one needs to calculate the optical paths of the rays from F to the screen. The following derivations are illustrated by Fig. 5. The angle β between the lines CB and CF is given by the equation

$$\sin\beta = \sin\theta'\left(-\frac{z'_F}{R}\cos\theta' - \sqrt{1-\frac{{z'_F}^2}{R^2}\sin^2\theta'}\right), \tag{4}$$

where θ' is the angle between the axis z' and the ray. Eq. (4) is obtained from the equation that expresses the tangent of θ'

$$\tan\theta' = \frac{x''_B}{-z'_F + z''_B} = \frac{R\sin\beta}{-z'_F - R\cos\beta} \ . \tag{5}$$

The incidence angle of the ray on the sphere is

$$\alpha = \theta' + \beta \, . \tag{6}$$

The refraction angle of the ray inside the sphere, from the refraction law, is

$$\alpha' = \arcsin\left(\frac{\sin\alpha}{n}\right), \tag{7}$$

where *n* is the refractive index of the water (here taken to be 1.3317). The deviation angle of the ray within the sphere from the axis *z*' has the value

$$\delta' = \theta' - (\alpha - \alpha') \, . \tag{8}$$

The angle between the ray and the *x*' axis is

$$\gamma = \beta + 2\delta' \, . \tag{9}$$

The total deviation of the ray from the *z*' axis, after refracting twice through the surface of the sphere, is

$$\delta = \delta' - (\alpha - \alpha') = \theta' - 2(\alpha - \alpha') \ . \tag{10}$$

In order to calculate the sampling grid for the interpolation of the optical path, we need the coordinates of the point W in the S system where the ray touches the screen. First we calculate those coordinates in the *S*" system

$$\begin{cases} x''_W = \Delta_1 / \Delta \\ z''_W = \Delta_2 / \Delta \end{cases}, \tag{11}$$

where

$$\begin{cases} \Delta_1 = \cos\xi\left(x''_G\cos\delta - z''_G\sin\delta\right) + z_W\sin\delta \\ \Delta_2 = z_W\cos\delta + \sin\xi\cos\varphi\left(x''_G\cos\delta - z''_G\sin\delta\right) \\ \Delta = \cos\delta\cos\xi - \sin\delta\sin\xi\cos\varphi \end{cases} . \tag{12}$$

Eqs. (11-12) were obtained by solving for x''_W and z''_W the system of 2 equations formed by

$$\frac{x''_W - x''_G}{z''_w - z''_G} = \tan\delta \tag{13}$$

and

$$z_W = -\sin\xi\cos\xi\, x''_W + \cos\xi\, z''_W \ . \tag{14}$$

Eq. (13) is the equation of the ray that exits the sphere at point *G* and reaches the screen at point *W* and Eq. (14) is obtained from the coordination transform equations from S" to S by setting $y''_W = 0$, which is true by definition. We already know z_W. Then we introduce Eqs. (11) in

$$\begin{cases} x_W = x_C + \cos\xi\cos\varphi\, x''_W + \sin\xi\, z''_W \\ y_W = \sin\varphi\, x''_W \end{cases} , \tag{15}$$

the remaining equations from the coordinate transform equations.

We separate the optical path in three parts, FB, BG and GW, (or d_1, d_2 and d_3) and their expressions are as follows

$$\begin{cases} d_1 = \sqrt{\left(z''_B - z'_F\right)^2 + x''^2_B} \\ d_2 = n\sqrt{\left(z''_G - z''_B\right)^2 + \left(x''_G - x''_B\right)^2} \\ d_3 = \sqrt{\left(z''_W - z''_G\right)^2 + \left(x''_W - x''_G\right)^2} \end{cases} . \tag{16}$$

The total optical path is, of course, their sum

$$d\left(x_W, y_W\right) = d_1 + d_2 + d_3 \ . \tag{17}$$

Using (15) and (17) we can calculate the interpolation function of the optical path as a function of the coordinates x_W and y_W. We need this interpolation function to calculate the interferogram.

4. RESULTS

In Fig. 6 one can do a side by side comparison between snapshots of the experimental interferogram from the observation screen and the calculated interferogram, at various times during the evaporation of the droplet. In the calculation we assumed a constant variation speed of the radius of the droplet. It is the consequence of assuming that the evaporation speed depends on the surface of the sphere only. The speed was adjusted in the calculations until we reached agreement with the variation speed of the fringes in the experiment. Namely this speed is v=0.14 μl/m^{2}s. The discrepancies between theory and experiment are probably due to the use of the geometric approximation, which may not be valid for the rays refracted close to tangency.

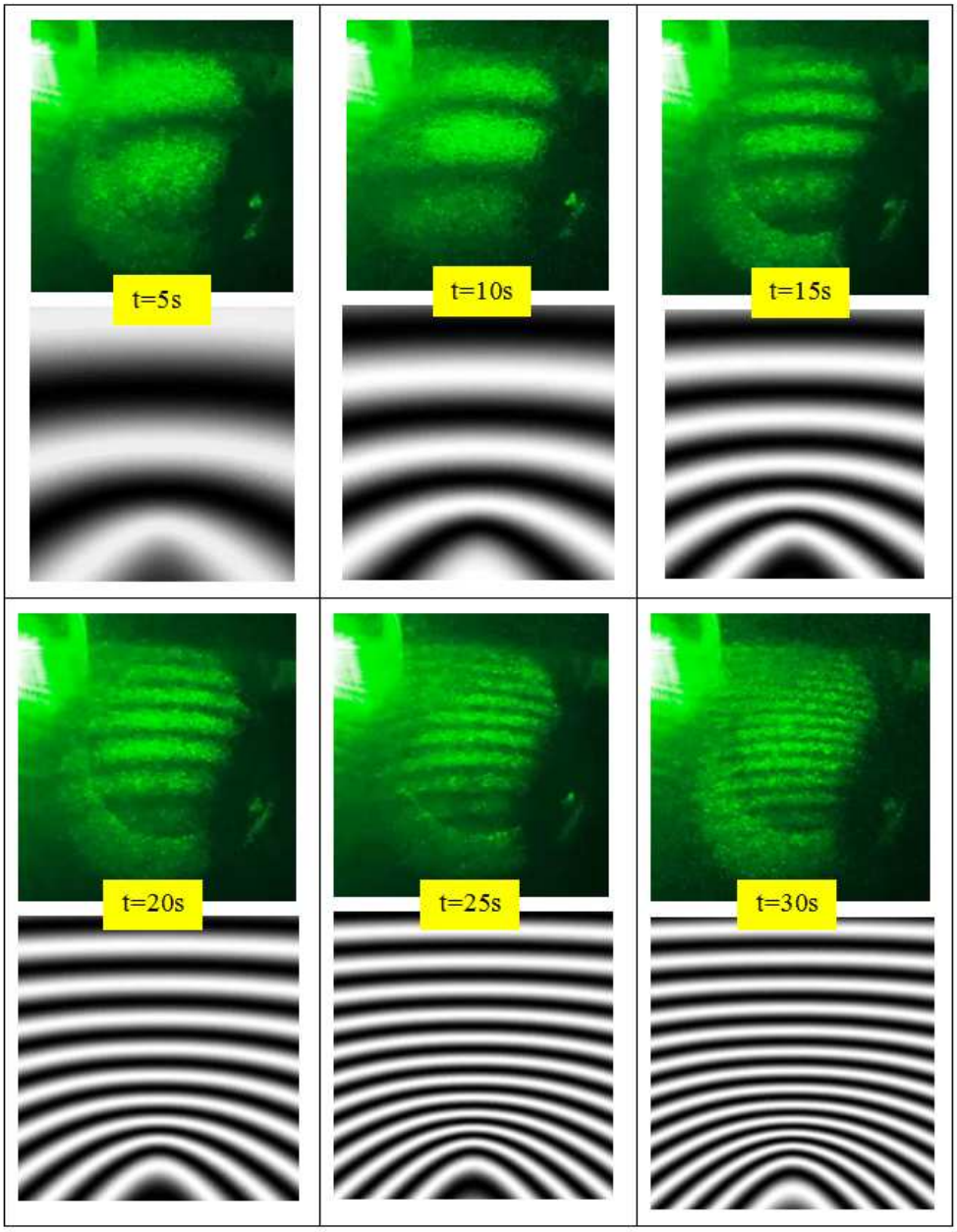

Fig. 6 – Side by side comparison between snapshots of the experimental (green) and the calculated (grey) interferograms taken at 5 seconds intervals during the evaporation.

5. CONCLUSIONS AND FUTURE WORK

The plane-parallel beams cannot be used to investigate interferometrically the dynamic processes inside a droplet, but divergent beams can, especially if there are some added features like real-time reconstructive holography and the use of holographic interferometry. Qualitative agreement between theory and experiment was achieved and an evaporation speed has been obtained by fitting. The geometric approximation is likely too strong, especially at large slant angles.

In order to make the comparison more quantitative, techniques such as fringe counting might be necessary.

The extension of the technique to the measurement of more complex phenomena, such as the perturbation of the droplet by inelastic or elastic interaction with a pulsed laser is straightforward, after precise fitting of the experiment and theory is accomplished.

Acknowledgments. This work was supported by Romanian Ministry of Education and Research, under Romanian National Nucleu Program LAPLAS VI – contract no. 16N/2019.

REFERENCES

1. D. Psaltis, S. R. Quake, and C. H. Yang, Nature **442**, 381–386 (2006).
2. V. R. Horowitz, D. D. Awschalom, and S. Pennathur, Lab. Chip. **8**, 1856–1863 (2008).
3. P. C. Logofătu, F. Garoi, M. Boni and M. L. Pascu, Rom. Rep. Phys. **72**, 403 (2020).
4. M. E. Riley and M. A. Gusinow, Appl. Opt. **16**, 2753-2756 (1977).
5. J. Luo, J. Bai, J. Zhang, C. Hou, K. Wang and X. Hou, Opt. Exp. **22**, 27921-27931 (2014).
6. A. Sima, P. Schiopu and P.C. Logofătu, 2017 9th International Conference on Electronics, Computers and Artificial Intelligence (ECAI), pp. 1-4 (2017).
7. A. Sima, P. Schiopu, M. Vladescu, B. M. Gavriloaia, F. Garoi, V. Damian, Lecture Notes of the Institute for Computer Sciences Social Informatics and Telecommunications Engineering **241**, 193-198 (2018).
8. P. C. Logofatu, F. Garoi, A. Sima, B. Ionita, D. Apostol, J. Optoelectron. Adv. M. **12**, 85 – 93 (2010).
9. W. J. Glantschnig and S.-H. Chen, Appl. Opt. **20**, 2499-2509 (1981).